# A Geometry Conforming, Isogeometric, Weighted Least Squares Method for the Neutron Transport Equation with Discrete Ordinate Angular Discretisation ($S_N$)

C. Latimer[a], J. Kópházi[a], M. D. Eaton[a], R. G. McClarren[b]

[a]*Nuclear Engineering Group*
*Department of Mechanical Engineering, Imperial College London*
*City and Guilds Building, Exhibition Road, South Kensington Campus, SW7 2AZ*
[b]*Department of Aerospace and Mechanical Engineering University of Notre Dame*
*Fitzpatrick Hall, Notre Dame, IN 46556*

**Abstract**

This paper presents the application of isogeometric analysis (IGA) to the spatial discretisation of the multi-group, source iteration compatible, weighted least squares (WLS) form of the neutron transport equation with a discrete ordinate ($S_N$) angular discretisation. The WLS equation is an elliptic, second-order form of the neutron transport equation that can be applied to neutron transport problems on computational domains where there are void regions present. However, the WLS equation only maintains conservation of neutrons in voided regions in the fine mesh limit. The IGA spatial discretisation is based up non-uniform rational B-spines (NURBS) basis functions for both the test and trial functions. In addition a methodology for selecting the magnitude of the weighting function for voided and near-void problems is presented. This methodology is based upon solving the first-order neutron transport equation over a coarse spatial mesh. The results of several nuclear reactor physics verification benchmark test cases are analysed. The results from these verification benchmarks demonstrate two key features. The first feature is that the magnitude of the error in the solution due to approximation of the geometry is greater than or equal to the magnitude of the error in the solution due to lack of conservation of neutrons. The second feature, the effect of the weighting factor on the solution, is investigated for a boiling water reactor (BWR) lattice that contains a burnable poison pincell. It is demonstrated that the smaller the area this weighting factor is active over, the closer the solution of the WLS equation is to the solution of the self adjoint angular flux (SAAF) equation. Finally, the methodology for selecting the magnitude of the weighting factor is shown to produce a suitable weighting factor for nuclear reactor physics problems containing voided regions. The finer the coarse solution of the first-order transport equation, the more suitable the weighting factor.

## 1. Introduction

Neutron transport problems that contain voided regions are typically solved using the first-order form of the neutron transport equation or Monte Carlo simulations [1]. Both of these

*Email address:* c.latimer15@imperial.ac.uk (C. Latimer)

methods can be combined in order to reduce the variance in the Monte Carlo solution. The adjoint first-order neutron transport is solved and the solution is used as an importance map for the Monte-Carlo algorithm [2, 3].

There are certain desirable numerical properties of the second-order form of the neutron transport equation compared to the first-order form. One important property is that when the second-order forms of the neutron transport equation are spatially discretised using a Bubnov-Galerkin finite element discretisation scheme they yield symmetric-positive definite (SPD) systems of linear equations. Such SPD matrix systems of linear equations can be solved using numerical efficient preconditioned conjugate gradient (CG) solution algorithms [4, 5]. However, traditional second-order forms of the neutron transport equation, such as the even-parity (EP) [6], odd-parity (OP), and self-adjoint angular flux (SAAF) [7] formulations can not be solved in voided regions. This is due to the reciprocal of the total macroscopic neutron cross-section that appears in these formulations.

There are two standard approaches to solving second order forms in voided regions. The first approach involves using a very low absorption macroscopic neutron cross-section within the void region [8]. This approach can lead to an increase in the condition number of the resultant system of linear equations and a potentially erroneous solution [9]. In particular, a flat neutron flux is often observed across the voided region [10]. Further research has been performed into improving the accuracy of this approach. These more complex methods involve solving the EP neutron transport equation several times whilst varying the value of the absorption macroscopic neutron cross-section used in the voided region. For example, the iteration and extrapolation methods proposed by Ackroyd [8, 11].

The other approach is to interface different forms of the neutron transport equation at the boundaries between voided and non-void regions. Work has been done on interfacing with both first-order [12] and other second-order forms [13, 14] of the neutron transport equations. These attempts often lead to a loss of symmetry of the system of linear equations which removes the possibility of using CG solvers.

A second-order form of the neutron transport equation recently proposed by Hansen et. al. is a source iteration compatible self-adjoint least squares method that is compatible with voided regions [15]. This allows the angular domain to be discretised using the $S_N$ method. The source iteration compatible LS equation removes the reciprocal of the total macroscopic neutron cross-section and therefore avoids the increase in condition number that is typically seen by second-order forms in near or fully voided regions. The cost of this is that conservation of neutrons is only guaranteed in the fine-mesh limit, something that is not unheard of in other void treatment methods [7].

Least squares (LS) formulations have been used in many areas of research such as: quantum electrodynamics [16], fluid mechanics [17], and biomolecular systems [18]. In particular, LS formulations of the neutron transport equation, where the scattering kernel is taken to be part of the transport operator, have been considered far back in the literature. LS based maximum principles for the first-order neutron transport equation were derived by Ackroyd and shown to be equivalent to the even and odd parity maximum principles [19]. Schofield expanded upon this work with a generalised LS form of the first-order neutron transport equation that is valid in voided regions. Second-order maximum variation principles were derived for both the steady state [20, 21] and time dependent neutron transport equation [22]. These maximum variational principles were applied to voided problems and shown to compare reasonably well to point kernel calculations, as well as the aforementioned interpolation and extrapolation methods [8].

Manteuffel & Ressel presented proofs for boundedness and coercivity of the LS formulation.

This means that the existence of a unique solution of the formulation can be proven using the Lax-Milgram theorem [23]. Error bounds, independent of cross-section, that held in the diffusion limit were also derived by applying a scaling to the neutron transport equation prior to the discretisation. The LS equation was solved in slab geometry discretised spatially and angularly using linear finite elements and spherical harmonics ($P_N$) respectively. Varin & Samba performed a similar analysis but compared the LS-$P_N$ equation to the diamond differenced first-order neutron transport equation with discrete ordinate ($S_N$) angular discretisation [24]. Both of the previous references [23, 24] only addressed isotropic scattering and Austin & Manteuffel produced a similar analysis but allowed for anisotropic scattering [25].

Chaudhry et. al. investigated adding an extra term to the LS formulation to provide extra accuracy in the evaluation of some quantity of interest (QoI) [26]. This was found to provide more accuracy in the evaluation of the QoI but produce a larger $L_2$ error for the solution as a whole for both diffusion and convection-diffusion equations. Drumm showed a simpler method of scaling the LS equation that allowed it to be solved accurately in thick diffusive media. This method was applied to one and two-dimensional void problems using finite elements with $P_N$ angular discretisation [27]. Ketelsen et. al. derived the LS equation from the first-order neutron transport equation formulated in one-dimensional (1D) spherical coordinates [28]. This removes the ray effects from the $S_N$ discretised solution at the cost of more strongly coupling all of the angular unknowns. However, all of the problems in the paper assume that there is no scattering.

Laboure et. al. presented the source iteration compatible LS equation angularly discretised with both $P_N$ and $S_N$ [29]. The effect that the lack of conservation of neutrons has on the source iteration compatible LS equations ability to solve criticality problems when compared to the SAAF equation for void free problems was highlighted. Furthermore, Laboure et. al presented a hybrid SAAF & conservative least squares (SAAF-CLS) formulation of the neutron transport equation that is valid in voided and near void regions, but whose variational form is not symmetric [13]. This methodology was shown to perform much better than the non-conservative LS formulation, and performed similarly to other void treated second-order forms of the neutron transport equation. Hammer et. al. derived a source iteration compatible weighted LS formulation by including a weighting operator [30]. This weighting operator was chosen so that in non-void regions the WLS formulation was identical to the SAAF formulation. In voided, or near-void, regions the formulation becomes more like Hansen's LS form [15]. Therefore, conservation of neutrons is not maintained in voided regions. However, the weighting term helps to restore causality to the formulation.

All of the aforementioned papers have spatially discretised the LS formulation using the finite element method (FEM). In this paper spatial discretisation will be performed using isogeometric analysis (IGA). IGA is a discretisation method that allows for the exact representation of geometries generated by commercial computer aided design (CAD) programs. This is achieved by using functions that are capable of exactly representing the known geometry as the basis functions to approximate the unknown solution. The functions chosen for this purpose in this paper are the non-uniform rational B-splines (NURBS). Since the geometry is taken directly from the CAD model, no meshing is required and there is no error in the geometric model, even on the coarsest level of refinement. In nuclear reactor physics problems this avoids numerical errors that are caused by inaccuracies in the representation of the volume and surface area of regions within the computational domain. For example, inaccuracies in representing the volume of regions within the computational domain leads to problems with preserving the fissile mass of fuel pins. Even when the volume of regions are exactly preserved, to machine precision, there may still be inaccuracies in the surface area, of these same regions, which can lead to numeri-

cal errors in representing the leakage of neutrons from fuel pins [31]. Furthermore, both spatial and polynomial refinement of the basis function space can be performed at run time allowing for smoother integration with adaptive mesh refinement (AMR) algorithms [32] and geometric multi-grid (GMG) solvers [33].

The aim of this paper in to investigate two issues. Firstly, the magnitude and effect of the error induced by the lack of conservation of neutrons will be investigated. Secondly, the benefits of the IGA discretisation methodology will be studied by comparing IGA against traditional FEM discretisation techniques. In section 2 the methodology of IGA is introduced. In section 3 the source iteration compatible weighted least squares (WLS) form of the neutron transport equation is derived. Furthermore, a procedure for choosing the weighting operator is discussed. Section 4 describes how the weak form of the WLS equation is spatially and angularly discretised using IGA and $S_N$ respectively. Finally the results of the WLS and LS equation applied to several nuclear reactor physics verification test cases are presented in section 5.

## 2. Isogeometric Analysis

Isogeometric analysis (IGA) is a numerical discretisation technique that uses basis functions capable of exactly representing the problem geometry as trial and test functions in the Bubnov-Galerkin weak form of a specified partial differential equation (PDE). The most widely used basis functions for IGA are the non-uniform rational B-spline (NURBS) functions. While other basis functions such as: T-splines [34], LR B-splines [35], and hierarchical B-splines [36] may be used NURBS are typically chosen as they are also employed by the majority of commercial CAD programs to build geometric models [37]. Therefore, using NURBS as the basis functions for IGA is a sensible choice as any CAD geometry model built using NURBS can be exactly represented by the IGA numerical program. This means that geometries that include conic sections in two-dimensions, and quadric surfaces in three-dimensions will have their volume and surface perfectly represented [37]. The theory, parameterisation, and generation of NURBS basis functions and objects will now be explained. NURBS are built upon basis splines (B-splines) so in order to describe NURBS functions B-splines will first be introduced. Furthermore, the topic of how general geometries are constructed from patches will be discussed.

### *2.1. B-spline basis functions*

B-splines are piece-wise polynomials that are defined over a knot vector. A knot vector is a sequence of non-decreasing real numbers $\Xi = \{\xi_1, \xi_2, \ldots, \xi_{m-1}, \xi_m\}$, with $\xi_i \in \mathbb{R}$. The B-spline basis functions over $\Xi$ are defined as:

$$N_{i,0}(\xi) = \begin{cases} 1 & \text{for } \xi \in [\xi_i, \xi_{i+1}), \\ 0 & \text{otherwise,} \end{cases}$$

$$N_{i,q}(\xi) = \frac{\xi - \xi_i}{\xi_{i+q} - \xi_i} N_{i,q-1}(\xi) + \frac{\xi_{i+q+1} - \xi}{\xi_{i+q+1} - \xi_{i+1}} N_{i+1,q-1}(\xi), \quad \text{for } q = 1, \ldots, p, \tag{1}$$

where if the expression $\frac{0}{0}$ occurs that term is assumed to be 0.

The multiplicity of knot $\xi_i$ is defined as the number of times it appears in $\Xi$ and is denoted $m_i$. B-spline functions are $C^{p-m_i}$ continuous at $\xi = \xi_i \in \Xi$ and $C^\infty$ at all other points. This is referred to as the inter-element continuity of a function. By repeatedly inserting knots the inter-element continuity of a B-spline function can be reduced as needed. For example, at a

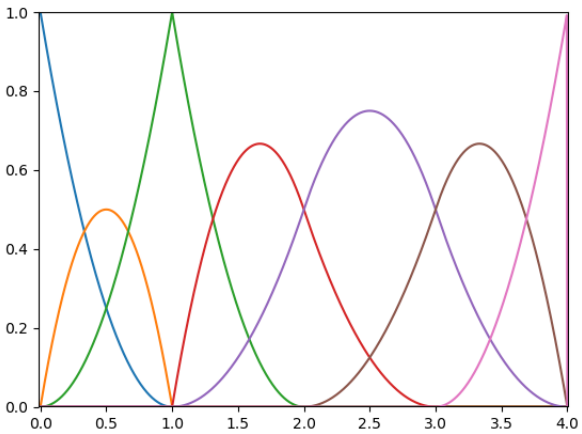


Figure 1: B-spline basis functions for the 2nd order open knot vector $\Xi = \{0, 0, 0, 1, 1, 2, 3, 4, 4, 4\}$

material discontinuity where there may be a strong gradient in the solution. If each knot is inserted $p$ times then all basis functions are $C^0$ over element boundaries similarly to traditional finite element basis functions.

A knot vector where the first and last knots are repeated $p + 1$ times is referred to as an open knot vector of order $p$. An open knot vector is capable of generating a set of B-spline basis functions of order $p$ that form a partition of unity over the entirety of $\Xi$ [38]. This means that the first and last B-spline basis functions are $C^0$ and therefore, interpolatory at $\xi_1$ and $\xi_m$ respectively. Some example two-dimensional B-spline functions can be seen in figure 2. The interpolatory nature of the B-spline functions can be seen in figure 2b where the maximum value of this functions is one.

Open knot vectors are the de facto standard for CAD models generated using NURBS [37] and are intuitive for designers to use due to the fact that the first and last basis functions are interpolatory. The partition of unity property leads to the strong convex hull property which makes the behaviour of B-spline objects more predictable when manipulating them in a commercial CAD program [39]. It will be seen later on that the NURBS basis functions inherit the strong convex hull property. From now on all knot vectors will be considered open knot vectors.

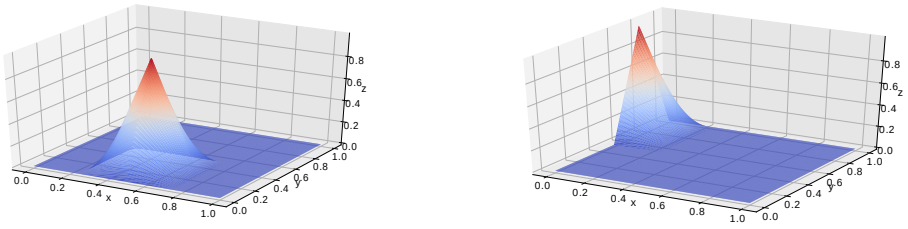


(a) The 8th B-spline basis function

(b) The 16th B-spline basis function

Figure 2: A selection of the two-dimensional B-spline basis functions generated over a unit square with the linear open knot vectors $\Xi_\xi = \Xi_\eta = \{0.0, 0.0, 0.25, 0.5, 0.75, 1.0, 1.0\}$

### 2.2. Non-uniform rational B-spline (NURBS) basis functions

Non-uniform rational B-splines (NURBS) are a generalisation of B-splines that, along with a knot vector $\Xi$, require the specification of a set of weights $\{w_i\}_{i=1}^{N} \in \mathbb{R}$, where $N$ is the number of basis functions. For an open knot vector $\Xi$ of order $p$, $N = m - (p + 1)$ where $m$ is the length of $\Xi$. The NURBS basis functions can then be generated using the following expression:

$$R_i^q(\xi) = \frac{N_{i,q}(\xi) w_i}{\sum_{j=1}^{N} N_{j,q}(\xi) w_j}, \text{ for } i = 1, 2, \ldots, N. \tag{2}$$

It is assumed that $w_i > 0$ for $\forall i$ as this means the NURBS functions inherit several useful properties from B-splines, such as non-negativity, high inter-element continuity, and the convex hull property [39]. Due to the partition of unity property of the B-spline basis functions it can be seen that the B-spline basis functions are a proper subset of the NURBS basis functions. This can be seen by setting $w_i = 1$ for $\forall i$ in which case expression (2) reads:

$$R_i^q(\xi) = N_{i,q}(\xi).$$

Furthermore, the NURBS basis functions generated over $\Xi$ form a basis for the rational, piecewise polynomials over $\Xi$.

### 2.3. NURBS curves, surfaces, and volumes

A NURBS object of dimension $d$ is defined as:

$$\mathbf{C}(\xi) = \sum_{i=1}^{N} R_i^q(\xi) \mathbf{B}_i, \tag{3}$$

where the set of $\mathbf{B}_i$'s $\in \mathbb{R}^3$ is known as the control points. In particular, $\mathbf{B}_i$ is the control point corresponding the the $i^{\text{th}}$ NURBS basis function. The function $\mathbf{C}(\xi)$ is known as the geometry map whose domain is the parametric domain $\hat{V}$ and whose range is the physical domain $V$. The $\mathbf{B}_i$'s define a bounding polygon that contains the physical domain $V$. This is known as the strong convex hull property and, as mentioned earlier, makes the design process more intuitive as well as preventing oscillations that may occur if high-order polynomials were used in an attempt to 'fit' the geometry [39]. This is known as Runge's phenomenon.

For higher dimensional problems the basis functions in equation (2) are not suitable and higher dimension basis functions are needed. Higher dimensional basis functions are generated using a tensor product structure. For example, in two-dimensions the NURBS functions are:

$$R_{i,j}^q(\xi, \eta) = \frac{N_{i,q}(\xi) N_{j,q}(\eta) w_{i,j}}{\sum_{l=1}^{M} \sum_{k=1}^{N} N_{k,q}(\xi) N_{l,q}(\eta) w_{l,k}}, \text{ for } i = 1, \ldots, N \text{ and } j = 1, \ldots M, \tag{4}$$

where each dimension is parameterised by a different knot vector $\Xi_\xi$ and $\Xi_\eta$. Once generated, the high dimension basis functions can be used in equation (3) to generate higher dimensional NURBS objects.

*2.4. NURBS patches*

Due to the tensor product structure used to generate higher-dimensional basis functions in expression (4), the parametric domain of a NURBS object is topologically equivalent to a hypercube. Therefore, in order to generate complex or multiply connected domains the concept of a NURBS patch is introduced.

A NURBS patch of order $p$ is a collection of open knot vectors, weights, and material coefficients. There are three main consequences of using NURBS patches. Firstly, as mentioned above, it allows the generation of geometries that are not topologically equivalent to a hypercube. Secondly the basis functions over the interfaces between patches are $C^0$-continuous. At first sight this appears to be a downside as it has been demonstrated that maintaining maximal continuity of NURBS basis functions within a NURBS patch leads to more accuracy per dof [40, 41]. However, since patches are regions with constant material properties, discontinuities in material properties can only occur at the interfaces between patches. Large gradients in the solution may appear at discontinuities in material properties and in order to represent these gradients it is ideal to have basis functions that are $C^0$ or even $C^{-1}$ continuous in order to avoid over-fitting the solution [37]. Therefore, the fact that the NURBS basis functions are $C^0$-continuous between NURBS patches is not as inefficient as it first seems. Finally, because the NURBS basis functions are $C^0$-continuous between NURBS patches, the patch-wise system matrices can be formed and assembled independently. This provides a convenient way in which to parallelise the assembly [37] and solution, via domain decomposition algorithms [42, 43], processes for the global system matrices.

Consistency of the NURBS mesh is enforced by matching the control points of neighbouring patches. While this leads to $C^0$-continuous basis functions, the final geometric model can have higher order continuity between patches [44]. This method of enforcing consistency, paired with the tensor product structure of the basis functions, means that refinement within a NURBS patch propagates to neighbouring patches. Local constraints can be applied in order to stop the propagation of refinement throughout the problem domain and is the subject of future work.

## 3. Derivation of weighted least squares (WLS) method

The steady-state (time-independent), first-order, energy-dependent, neutron transport equation is given by:

$$\mathbf{\Omega} \cdot \nabla \psi(\mathbf{r}, \mathbf{\Omega}, E) + \sigma_t(\mathbf{r}, E)\psi(\mathbf{r}, \mathbf{\Omega}, E) = Q_{\text{scatter}}(\mathbf{r}, \mathbf{\Omega}, E) + Q_{\text{ext}}(\mathbf{r}, \mathbf{\Omega}, E), \tag{5}$$

where

$$Q_{\text{scatter}}(\mathbf{r}, \mathbf{\Omega}, E) = \int_0^\infty \int_{4\pi} \sigma_s\left(\mathbf{r}, \mathbf{\Omega}' \rightarrow \mathbf{\Omega}, E' \rightarrow E\right) \psi(\mathbf{r}, \mathbf{\Omega}', E') d\mathbf{\Omega}' dE', \tag{6}$$

and $Q_{\text{ext}}(\mathbf{r}, E)$ consists of neutron fission and extraneous (fixed) sources. Furthermore, the total source is defined as:

$$Q(\mathbf{r}, \mathbf{\Omega}, E) = Q_{\text{scatter}}(\mathbf{r}, \mathbf{\Omega}, E) + Q_{\text{ext}}(\mathbf{r}, \mathbf{\Omega}, E).$$

The transport operator is defined as $\mathcal{L} = \mathbf{\Omega} \cdot \nabla + \sigma_t(\mathbf{r}, E)$ such that equation (5) can be written as:

$$\mathcal{L}\psi(\mathbf{r}, \mathbf{\Omega}, E) = Q(\mathbf{r}, \mathbf{\Omega}, E). \tag{7}$$

By considering the inner product $\int_V \int_{4\pi} \int_0^\infty dE d\mathbf{\Omega} d\mathbf{r}$ an expression for the adjoint transport operator $\mathcal{L}^\dagger$ can be derived by solving the equation:

$$\int_V \int_{4\pi} \int_0^\infty u(\mathbf{r}, \mathbf{\Omega}, E) \mathcal{L} v(\mathbf{r}, \mathbf{\Omega}, E) dE d\mathbf{\Omega} d\mathbf{r} = \int_V \int_{4\pi} \int_0^\infty \mathcal{L}^\dagger u(\mathbf{r}, \mathbf{\Omega}, E) v(\mathbf{r}, \mathbf{\Omega}, E) dE d\mathbf{\Omega} d\mathbf{r}. \quad (8)$$

This yields the following expression for the adjoint transport operator:

$$\mathcal{L}^\dagger = -\mathbf{\Omega} \cdot \nabla + \sigma_t(\mathbf{r}, E). \quad (9)$$

For this derivation the following notation for the inner product over the spatial domain is introduced:

$$\left(u, v\right)_V = \int_V uv d\mathbf{r},$$
$$\left\langle u, v\right\rangle_\Gamma = \int_\Gamma uv d\mathbf{r_s},$$

where $V$ is the physical domain, $\Gamma$ is the boundary of $V$, and $\mathbf{r} \in V$ and $\mathbf{r_s} \in \Gamma$. Then the first-order neutron transport equation in operator form, see equation (7), is operated on by $\mathcal{L}^\dagger \mathcal{W}$ yielding:

$$\mathcal{L}^\dagger \mathcal{W} \mathcal{L} \psi(\mathbf{r}, \mathbf{\Omega}, E) = \mathcal{L}^\dagger \mathcal{W} Q(\mathbf{r}, \mathbf{\Omega}, E), \quad (10)$$

where $\mathcal{W}$, known as the weighting operator, is to be chosen later on. This operator equation can be written algebraically. The left hand side (LHS) and right hand side (RHS) of equation (10) are considered separately yielding:
LHS:

$$\begin{aligned} \mathcal{L}^\dagger \mathcal{W} \mathcal{L} \psi &= \left(-\mathbf{\Omega} \cdot \nabla + \sigma_t\right) \mathcal{W} \left(\mathbf{\Omega} \cdot \nabla \psi + \sigma_t \psi\right) \\ &= \left(-\mathbf{\Omega} \cdot \nabla + \sigma_t\right) \left(\mathcal{W}\mathbf{\Omega} \cdot \nabla \psi + \mathcal{W}\sigma_t \psi\right) \\ &= -\mathbf{\Omega} \cdot \nabla \left(\mathcal{W}\mathbf{\Omega} \cdot \nabla \psi\right) - \mathbf{\Omega} \cdot \nabla \left(\mathcal{W}\sigma_t \psi\right) + \sigma_t \mathcal{W}\mathbf{\Omega} \cdot \nabla \psi + \mathcal{W}\sigma_t^2 \psi, \end{aligned} \quad (11)$$

RHS

$$\mathcal{L}^\dagger \mathcal{W} Q = \left(-\mathbf{\Omega} \cdot \nabla + \sigma_t\right) \mathcal{W} Q = -\mathbf{\Omega} \cdot \nabla \mathcal{W} Q + \sigma_t \mathcal{W} Q. \quad (12)$$

It is noted that the application of the product rule to the LHS would result in the combination of the second and third terms in equation (11). However, this requires that both functions be differentiable. Since $\mathcal{W}$ has not been chosen yet nothing can be said about its differentiability. Furthermore, $\sigma_t$ is allowed to be discontinuous at patch boundaries. Since both functions are not differentiable over the domain the product rule is not applicable here. Despite not being allowed, its application would yield the same weak form. This derivation continues without any application of the product rule. Equating sides gives:

$$-\mathbf{\Omega} \cdot \nabla \left(\mathcal{W}\mathbf{\Omega} \cdot \nabla \psi\right) - \mathbf{\Omega} \cdot \nabla \left[\left(\mathcal{W}\sigma_t\right)\psi\right] + \sigma_t \mathcal{W}\mathbf{\Omega} \cdot \nabla \psi + \mathcal{W}\sigma_t^2 \psi = \left(\sigma_t - \mathbf{\Omega} \cdot \nabla\right) \mathcal{W} Q, \quad (13)$$

which is then multiplied by a test function $v$ and integrated over the entire spatial domain to give the weak form:

$$\begin{aligned} &-\left(\mathbf{\Omega} \cdot \nabla \left(\mathcal{W}\mathbf{\Omega} \cdot \nabla \psi\right), v\right)_V - \left(\mathbf{\Omega} \cdot \nabla \left(\mathcal{W}\sigma_t \psi\right), v\right)_V + \left(\sigma_t \mathcal{W}\mathbf{\Omega} \cdot \nabla \psi, v\right)_V + \left(\mathcal{W}\sigma_t^2 \psi, v\right)_V \\ &= \left(\mathcal{W} Q, \sigma_t v\right)_V - \left(\mathbf{\Omega} \cdot \nabla \mathcal{W} Q, v\right)_V. \end{aligned} \quad (14)$$

Performing integration by parts on the first and second terms on the left hand side and the second term on the right hand side gives:

$$\begin{aligned}&\Big(\mathcal{W}\boldsymbol{\Omega}\cdot\nabla\psi,\boldsymbol{\Omega}\cdot\nabla v\Big)_V+\Big(\mathcal{W}\boldsymbol{\Omega}\cdot\nabla\psi,\sigma_t v\Big)_V+\Big(\mathcal{W}\sigma_t\psi,\boldsymbol{\Omega}\cdot\nabla v\Big)_V+\Big(\mathcal{W}\sigma_t\psi,\sigma_t v\Big)_V\\&-\Big\langle w\boldsymbol{\Omega}\cdot\nabla\psi,(\boldsymbol{\Omega}\cdot\mathbf{n})\,v\Big\rangle_\Gamma-\Big\langle\mathcal{W}\sigma_t\psi,(\boldsymbol{\Omega}\cdot\mathbf{n})\,v\Big\rangle_\Gamma=\\&\Big(\mathcal{W}Q,\sigma_t v\Big)_V+\Big(\mathcal{W}Q,\boldsymbol{\Omega}\cdot\nabla v\Big)_V-\Big\langle\mathcal{W}Q,(\boldsymbol{\Omega}\cdot\mathbf{n})\,v\Big\rangle_\Gamma,\end{aligned}\tag{15}$$

which can be simplified to:

$$\begin{aligned}&\Big(\mathcal{W}\boldsymbol{\Omega}\cdot\nabla\psi,\boldsymbol{\Omega}\cdot\nabla v+\sigma_t v\Big)_V+\Big(\mathcal{W}\sigma_t\psi,\boldsymbol{\Omega}\cdot\nabla v+\sigma_t v\Big)_V-\Big\langle\mathcal{W}\boldsymbol{\Omega}\cdot\nabla\psi+\mathcal{W}\sigma_t\psi,(\boldsymbol{\Omega}\cdot\mathbf{n})\,v\Big\rangle_\Gamma\\=&\Big(\mathcal{W}Q,\boldsymbol{\Omega}\cdot\nabla v+\sigma_t v\Big)_V-\Big\langle\mathcal{W}Q,(\boldsymbol{\Omega}\cdot\mathbf{n})\,v\Big\rangle_\Gamma.\end{aligned}\tag{16}$$

The boundary terms can be removed as they satisfy the first-order neutron transport equation given in equation (5), leaving:

$$\Big(\mathcal{W}\boldsymbol{\Omega}\cdot\nabla\psi,\boldsymbol{\Omega}\cdot\nabla v+\sigma_t v\Big)_V+\Big(\mathcal{W}\sigma_t\psi,\boldsymbol{\Omega}\cdot\nabla v+\sigma_t v\Big)_V=\Big(\mathcal{W}Q,\boldsymbol{\Omega}\cdot\nabla v+\sigma_t v\Big)_V.\tag{17}$$

The removal of the boundary integral terms leaves no way to satisfy natural boundary conditions. Therefore, these are implemented weakly by introducing an additional term with a penalty parameter, $c$ into equation (17). The final weak form is then:

$$\begin{aligned}&\Big(\mathcal{W}\boldsymbol{\Omega}\cdot\nabla\psi,\boldsymbol{\Omega}\cdot\nabla v+\sigma_t v\Big)_V+\Big(\mathcal{W}\sigma_t\psi,\boldsymbol{\Omega}\cdot\nabla v+\sigma_t v\Big)_V+c\int_{\Gamma^-}\mathcal{W}v|\boldsymbol{\Omega}\cdot\mathbf{n}|\,(\psi-F)\,d\mathbf{r_s}\\=&\Big(\mathcal{W}Q,\boldsymbol{\Omega}\cdot\nabla v+\sigma_t v\Big)_V,\end{aligned}\tag{18}$$

where $\Gamma^-=\{\Gamma\mid\boldsymbol{\Omega}\cdot\mathbf{n}<0\}$ and $F(\mathbf{r},\boldsymbol{\Omega},E)$, defined for $\mathbf{r_s}\in\Gamma^-$, is a function that represents the boundary conditions. For example:

- $F=0\Rightarrow$ vacuum boundary
- $F=\psi(\mathbf{r},\boldsymbol{\Omega}_R,E)\Rightarrow$ reflective boundary, where $\boldsymbol{\Omega}_R$ is the angle of specular reflection of $\boldsymbol{\Omega}$
- $F=\zeta(\mathbf{r},\boldsymbol{\Omega},E)\Rightarrow$ incoming boundary source.

The penalty parameter $c$ is taken to be:

$$c=\max\left(\sigma_t,\frac{1}{h}\right),$$

where $h$ is a measurement of element size, taken here to be the largest distance between successive knots in a patch. This is suggested by Laboure in order to ensure that the LS formulation is consistent with the SAAF formulation, that is they differ only by their discretisation error when $c=\sigma_t$ [45].

Equation (18) with $\mathcal{W} = 1$ is the source iteration compatible LS form presented by Hansen et. al [15]. A non unit weighting factor gives the source iteration compatible weighted LS (WLS) form given by Hammer et. al. [30].

The weighting factor suggested by Hammer et. al. [30] is:

$$\mathcal{W} = \min\left(\frac{1}{\sigma_t}, w_{\max}\right), \tag{19}$$

where $w_{\max} \in \mathbb{R}$ is the maximum weight. In non-void regions $\mathcal{W} = \frac{1}{\sigma_t}$ implies that the WLS equation will be equivalent to the SAAF equation, up to boundary conditions. This means that that the WLS equation conserves neutrons in non-void regions, unlike Hansen's LS equation. However, in near-void and voided regions $\frac{1}{\sigma_t} \to \infty$ meaning equation (18) will tend towards a singularity. When this would happen the weighting factor becomes $w_{\max}$, the singularity is avoided but at the cost of losing conservation of neutrons in near-void and voided regions.

### *3.1. Choice of the weighting operator $\mathcal{W}$*

In the original WLS paper by Hammer et. al. [30] the dependence of the solution of the WLS equation on the value $w_{\max}$ was analysed. It was suggested that the optimal value of $w_{\max}$ is independent of mesh size. Furthermore, it is suggested that $w_{\max}$ should be angularly dependent to account for the fact that neutrons streaming in different directions may travel different distances in a given voided region. A strategy, based on the assumption that $w_{\max}$ is independent of the mesh size, for choosing an appropriate value of $w_{\max}$ is presented here. The algorithm, which requires a code capable of solving the first-order neutron transport equation, is presented in figure 3 and is also explained below.

First a quantity of interest (QoI) is chosen, for example: the $K_{\text{eff}}$, a reaction rate over part of the domain, or a detector response at a given location. Once this has been selected the first-order neutron transport equation can be solved for the given problem and the QoI recorded, denoted here by $Q_f$. In this paper, the WLS equation is spatially and angularly discretised using IGA and $S_N$ respectively. Therefore, a first-order neutron transport IGA-$S_N$ code is used to ensure that no errors caused by geometric approximation or differing angular discretisation enter the problem here.

An interval $\mathcal{I} \subset \mathbb{R}$ is selected and a set of weights $w_i \in \mathcal{I}$ is chosen. This set of weights is denoted $\mathcal{P}$. The WLS equation is then solved for each $w_i \in \mathcal{P}$ over a coarse mesh and the QoI recorded, denoted here by $Q_{w_i}$. If there exists a $Q_{w_i}$ such that $|Q_f - Q_{w_i}| < \epsilon$, where $\epsilon$ is is some tolerance, then $w_{\max} = w_i$ is chosen. If such a $w_i$ is not found then a new $\mathcal{I}$ and $\mathcal{P}$ are chosen until a suitable weighting factor is found. In accordance with the assumption that $w_{\max}$ should be almost independent of mesh size, this procedure should give a good value of $w_{\max}$ for a highly spatially refined solution of the WLS neutron transport equation with the same level of angular discretisation.

One potential issue with this algorithm is related to the error in the QoI calculated from the first-order neutron transport solution, $Q_f$. Since $Q_f$ is calculated over a coarse mesh there will be some error in $Q_f$ relative to the exact answer, $Q_f^e$. It would be ideal to minimise the error in the QoI using $|Q_f^e - Q_{w_i}| < \epsilon$. However, the exact solution $Q_f^e$ is not available so the expression $|Q_f - Q_{w_i}|$ is used. Therefore, it would be beneficial to minimise $|Q_f^e - Q_f|$ to ensure that $Q_{w_i}$ is being matched with a value of $Q_f$ that is sufficiently close to the exact solution $Q_f^e$. Minimising $|Q_f^e - Q_f|$ implies that the mesh for the first-order neutron transport calculation should be highly refined. This causes two issues with respect to the run time of the algorithm suggested here.

Firstly, the finer the 'coarse' first-order neutron transport calculation, the finer the 'coarse' WLS calculation must be in order to find the value of $w_{\max}$ that produces a matching QoI. Therefore, the finer the 'coarse' mesh is, the longer the algorithm takes to run.

Secondly, if it is possible to obtain fine mesh solutions of the first-order neutron transport equation in a reasonable time for voided problems then this algorithm, along with the WLS equation, would be unnecessary. If it is not possible to obtain fine mesh solutions of the first-order neutron transport equation in a reasonable time then the computational cost of applying this algorithm for a fine 'coarse' mesh would be too high. Therefore, a coarse 'coarse' mesh should be used. The effect of the fineness of the 'coarse' mesh will be investigated in section 5.

## 4. Spatial and angular discretisation of the weak form of the WLS neutron transport equation

### *4.1. Discrete ordinate ($S_N$) discretisation of the WLS neutron transport equation*

In this paper the angular variable is discretised using the discrete ordinates ($S_N$) method. The $S_N$ method is a quadrature rule that can be used to evaluate angular integrals as follows:

$$\int_{4\pi} f(\mathbf{\Omega}) d\mathbf{\Omega} \approx \sum_{m=1}^{N} w_m f(\mathbf{\Omega}_m). \tag{20}$$

A quadrature set defining the quadrature weights and directions $\{w_m, \mathbf{\Omega}_m\}_{m=1}^N$ must be chosen. Some examples of suitable angular quadrature sets are level-symmetric quadrature sets, and Legendre-Chebyshev quadrature sets.

In order to find the scalar neutron flux the weak form is evaluated and solved for each angle $\mathbf{\Omega}_m \in \{\mathbf{\Omega}_m\}_{m=1}^N$. Then the quadrature rule can be used to recover the scalar neutron flux from the angular neutron fluxes as follows:

$$\phi(\mathbf{r}, E) = \int_{4\pi} \psi(\mathbf{r}, \mathbf{\Omega}, E) d\mathbf{\Omega} = \sum_{m=1}^{N} w_m \psi(\mathbf{r}, \mathbf{\Omega}_m, E) = \sum_{m=1}^{N} w_m \psi_m(\mathbf{r}, E), \tag{21}$$

where $\psi_m(\mathbf{r}, E) \coloneqq \psi(\mathbf{r}, \mathbf{\Omega}_m, E)$. This means that in order to use expression (21), equation (18) must be solved for $\forall \mathbf{\Omega}_m$. That is:

$$\langle \mathcal{W}\mathcal{L}_m\psi_m, \mathcal{L}_m v\rangle + \int_{\Gamma_m^-} c\mathcal{W}v \left(\mathbf{\Omega}_m \cdot \mathbf{n}\right) \left(\psi_m - F\left(\mathbf{r}, \mathbf{\Omega}_m\right)\right) d\mathbf{r}_\mathbf{s} = \langle \mathcal{W}Q_m, \mathcal{L}_m v\rangle . \tag{22}$$

where $\mathcal{L}_m \coloneqq \mathbf{\Omega}_m \cdot \nabla + \sigma_t(\mathbf{r}, E)$ and $\Gamma_m^- = \{\Gamma \mid \mathbf{\Omega}_m \cdot \mathbf{n} < 0\}$.

In Morel & McGhees paper [7] it is noted that the SAAF-$S_N$ formulation can be derived either directly, by evaluating the final weak form in a direction $\mathbf{\Omega}_m$, or indirectly by evaluating the strong form in a direction $\mathbf{\Omega}_m$ and then proceeding to derive the weak form. It is stated that these methods lead to the same set of equations. This is also the case for the WLS-$S_N$ formulation. This can be seen by defining $\mathcal{L}_m = \mathbf{\Omega}_m \cdot \nabla + \sigma_t(\mathbf{r}, E)$ and $\mathcal{L}_m^\dagger = -\mathbf{\Omega}_m \cdot \nabla + \sigma_t(\mathbf{r}, E)$. Then it can be noted that equation (10) evaluated at $\mathbf{\Omega} = \mathbf{\Omega}_m$ gives

$$\mathcal{L}_m^\dagger \mathcal{W}\mathcal{L}_m\psi_m(\mathbf{r}, E) = \mathcal{L}_m^\dagger \mathcal{W}Q_m(\mathbf{r}, E).$$

Following through with the same weak form procedure specified in section 3 yields a weak form that is equivalent to equation (22).

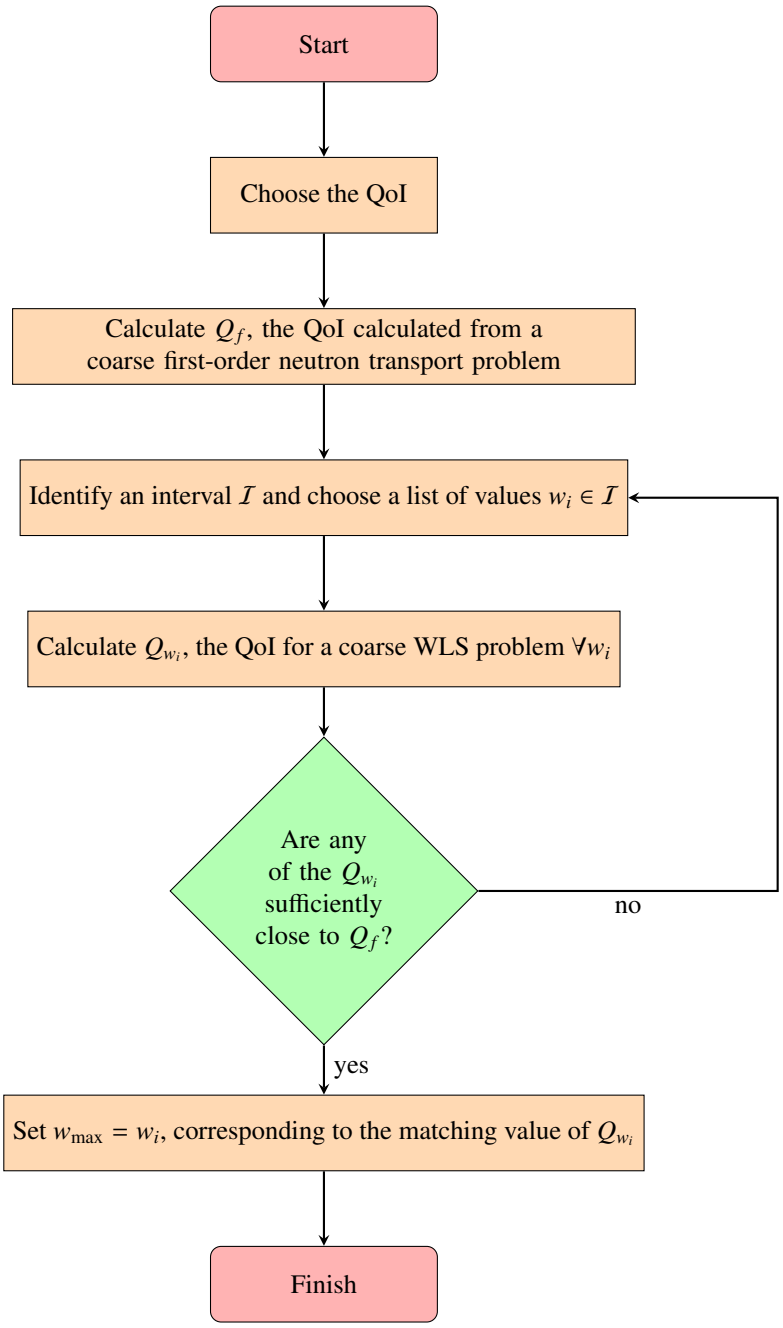


Figure 3: The algorithm for choosing a value of $w_{\max}$ based upon a solution of the first-order neutron transport equation.

*4.2. IGA spatial discretisation of the weak form of the WLS neutron transport equation*

The IGA discretisation of the weak form of the WLS begins by expanding the spatial dependence of the solution as a linear combination of trial functions:

$$\psi_m(\mathbf{r}, E) = \sum_{i=1}^{\infty} d_{i,m}(E) v_i(\mathbf{r}), \tag{23}$$

where the $d_{i,m}(E)$ are referred to as the control variables. The $v_i \in T_R$ are referred to as the trial functions and belong to the infinite dimensional trial function space:

$$T_R = \left\{ v \mid v \in H^1(V),\ v|_{\Gamma_D} = g \right\}, \tag{24}$$

where $H^1(V)$ is the Sobolev space $W_2^1(V)$ over the domain V [46]. The condition $v|_{S_D} = g$ allows for the implementation of essential boundary conditions, such as a Dirichlet boundary condition: $\psi(\mathbf{r}) = g$ for $\mathbf{r} \in \Gamma_D$ [37]. A test function $w$ is chosen to belong to another infinite dimensional space:

$$T_E = \left\{ w \mid w \in H^1(V),\ w|_{\Gamma} = 0 \right\}, \tag{25}$$

which is known as the test function space. The condition $w|_{\Gamma} = 0$ is enforced so that the test functions do not interfere with the essential boundary conditions.

In order to provide closure to expression (23) the expansion must be truncated. In order to achieve this, finite dimensional analogues of the trial and test function spaces are defined:

$$T_R^h = \left\{ v_i^h \mid v_i^h \in H^1(V),\ v_i^h|_{\Gamma_D} = g,\ \text{for } i \in [1, N] \right\},$$
$$T_E^h = \left\{ w_i^h \mid w_i^h \in H^1(V),\ w_i^h|_{\Gamma} = 0,\ \text{for } i \in [1, N] \right\},$$

and the solution can then be approximated by a truncated expansion:

$$\psi_m(\mathbf{r}, E) \approx \psi_m^h(\mathbf{r}, E) = \sum_{i=1}^{N} d_{i,m}(E) v_i^h(\mathbf{r}). \tag{26}$$

The Bubnov-Galerkin IGA discretisation is then formulated by making the choice $v_i(\mathbf{r}) = R_i^q(\mathbf{r}) \in T_R^h$ and $w_j(\mathbf{r}) = R_j^q(\mathbf{r}) \in T_E^h$. The truncated expansion of the angular flux given by expression (26) is substituted into the weak form given in equation (22). Furthermore, $w_j = R_j^q$ is substituted into equation (22) in place of $v$ yielding:

$$\begin{aligned} \sum_{i=1}^{N} d_{i,m} \Bigg[ \int_V (\mathcal{W}\boldsymbol{\Omega}_m \cdot \nabla R_i + \mathcal{W}\sigma_t R_i)(\boldsymbol{\Omega}_m \cdot \nabla R_j + \sigma_t R_j) d\mathbf{r} + c \int_{\Gamma_m^-} |\boldsymbol{\Omega}_m \cdot \mathbf{n}| \mathcal{W} R_j (R_i - F) d\mathbf{r}_\mathbf{s} \Bigg] \\ = \int_V \mathcal{W} Q_m (\boldsymbol{\Omega}_m \cdot \nabla R_j + \sigma_t R_j) d\mathbf{r}. \end{aligned} \tag{27}$$

This global bilinear form can be split into the summation of local bilinear forms computed over

knot spans as follows:

$$\begin{aligned}
&\sum_{i=1}^{N} d_{i,m} \sum_{p=1}^{P} \sum_{e=1}^{e_p} \int_{V_e} (\mathcal{W}\boldsymbol{\Omega}_m \cdot \nabla R_i + \mathcal{W}\sigma_t R_i)(\boldsymbol{\Omega}_m \cdot \nabla R_j + \sigma_t R_j) d\mathbf{r} \\
&+ \sum_{i=1}^{N} d_{i,m} \sum_{p=1}^{P} \sum_{b=1}^{b_p} c \int_{\Gamma^-_{m,b}} |\boldsymbol{\Omega}_m \cdot \mathbf{n}| \mathcal{W} R_j (R_i - F) d\mathbf{r}_\mathbf{s} \\
&= \sum_{p=1}^{P} \sum_{e=1}^{e_p} \int_{V_e} \mathcal{W} Q_m (\boldsymbol{\Omega}_m \cdot \nabla R_j + \sigma_t R_j) d\mathbf{r}.
\end{aligned} \tag{28}$$

where $P$ is the number of patches in the domain, $e_p$ is the number of knot spans in patch $p$, $b_p$ is the number of knot spans on the external boundary of patch $p$, $V_e$ is the volume of knot span $e$, and $\Gamma^-_{m,b}$ is the external surface of knot span $b$ such that $\boldsymbol{\Omega}_m \cdot \mathbf{n} < 0$.

## 5. Problems

The nuclear reactor physics and radiation shielding verification benchmark test cases in this section have been chosen to investigate two topics.

Firstly, the solutions of FE and IGA discretisation methods are compared for several nuclear reactor physics extraneous (fixed) source and fission source problems. These problems will illustrate the magnitude of errors that are incurred when the two-dimensional geometries are approximated by quadrilaterals, as is the case in traditional FE discretisations. Whilst volume or surface area preservation techniques can be applied to FE meshes, it is impossible to accurately preserve both the fissile mass and the surface area of conic sections in 2D and quadric surfaces in 3D using standard higher order FE basis functions. This is due to the fact that these basis functions are not able to represent conic sections and quadric surfaces exactly. However, the basis functions associated with the IGA method are chosen such that they are able to exactly represent both the volume and surface area of these geometries exactly.

Using curvilinear high order isoparametric FEs to approximate pincell geometries has been investigated for the first-order neutron transport equation [47]. Furthermore, comparisons between curvilinear high order isoparametric FEs and IGA have been performed for the first-order neutron transport equation [32] and the multigroup diffusion equation [41]. It was seen that, even with a similar number of elements per pincell, the error in detector response for FE solutions could be over one order of magnitude greater than similarly discretised IGA solutions. Since isoparametric FEs preserve neither volume or surface area exactly for a pincell, in this paper volume preserved higher order isoparametric finite elements with straight sides are investigated. This means that the error in approximating the surface area of the geometry is easily determined and fissile mass will be preserved exactly.

The second issue investigated in this section is the lack of conservation of neutrons over the entire domain inherent in the LS and WLS methods. Several of the nuclear reactor physics and radiation shielding test cases will highlight the errors associated with this property. Furthermore, the effect of the magnitude of $w_{\max} \in \mathbb{R}$ on the solution of the WLS equation will be investigated for voided and non-void problems.

The continuous IGA-WLS spatial discretisation method developed in this paper has been implemented with a modified version of the Fortran code ICARUS (Isogeometric Continuous

| Region | Macroscopic neutron cross-section ($cm^{-1}$) | | Extraneous source strength ($cm^{-3}.s^{-1}$) |
|---|---|---|---|
| | $\sigma_t$ | $\sigma_a$ | $Q$ |
| Fuel | 0.764 | 0.367 | 1.0 |

Table 1: Material cross-sections for the bare fuel pin extraneous (fixed) source nuclear reactor physics verification test case.

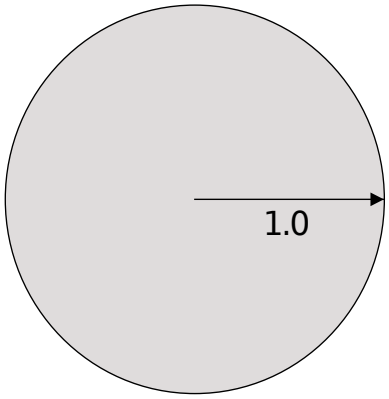


Figure 4: Geometry for the bare pin extraneous (fixed) source nuclear reactor physics verification benchmark test case. All of the boundary conditions are vacuum.

self-Adjoint Radiation Using Splines). ICARUS is used to generate the WLS-$S_N$, LS-$S_N$, and the SAAF-$S_N$ results in this paper for both IGA and FE discretisations. Inferno is a first-order neutron transport code with local refinement capabilities [32, 48, 49]. It is a discontinuous IGA-$S_N$ code and is used to generate reference solutions to both voided and non-voided nuclear reactor physics verification benchmark test cases.

### *5.1. Bare fuel pin extraneous (fixed) source nuclear reactor physics verification benchmark test case*

This nuclear reactor physics test case is taken from work by Hall et. al. [31]. The verification test case is comprised of a bare fuel pin with an extraneous (fixed) source. The macroscopic cross-section data and the extraneous (fixed) source strength are displayed in table 1 and the geometry in figure 4. It has been noted the the LS equation lacks conservation of neutrons except in the fine mesh limit. However, it is hard to say where the fine mesh limit is. In an attempt to quantify the magnitude of the error that lack of conservation of neutrons may induce in the solution the bare pin test case has been run with several different discretisation techniques. The LS and SAAF equations have been spatially discretised using FEs, volume-preserved FEs, and IGA and angularly discretised using an $S_{10}$ quadrature set. The results are displayed in figure 5.

Figure 5a shows the SAAF and LS equations discretised using quadratic, non volume-preserved FEs. It can be observed that the SAAF and LS solutions seem to agree, that is the error caused by the lack of conservation of neutrons is small compared to the error caused by approximat-

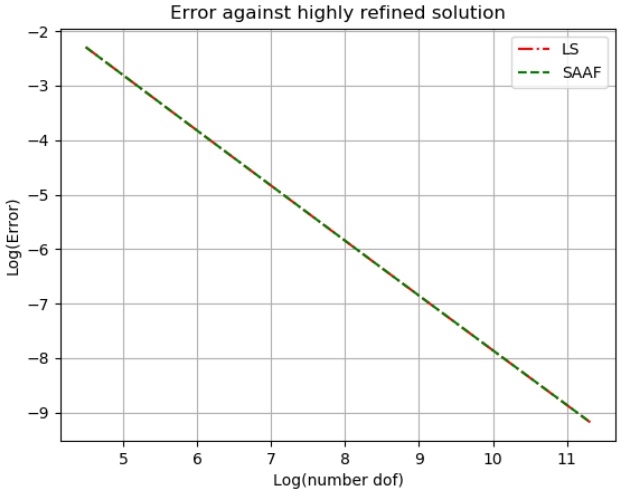


(a) FEM no volume preservation

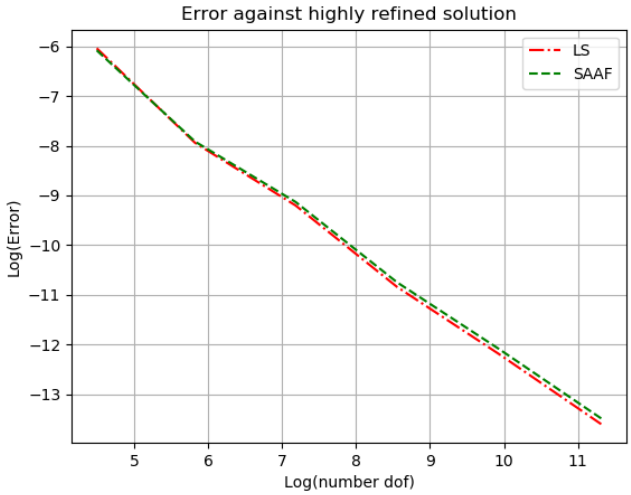


(b) FEM volume preservation

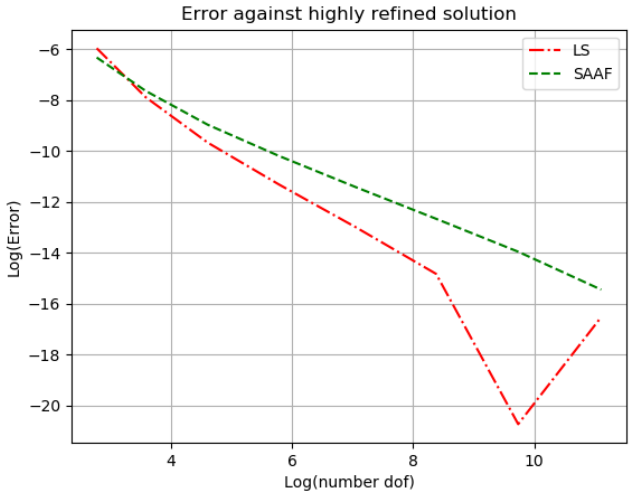


(c) IGA

Figure 5: Errors in the integral of the flux over the domain for the bare pin extraneous (fixed) source nuclear reactor physics verification test case.

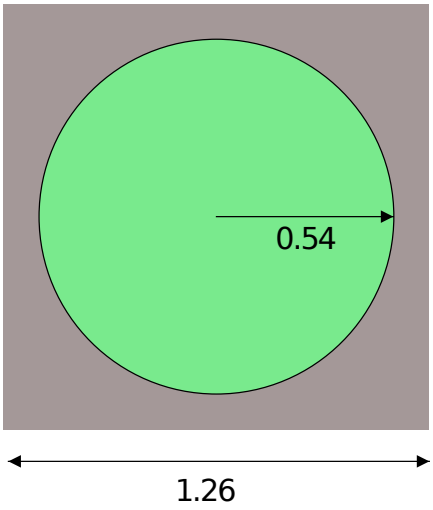


Figure 6: Geometry for the seven group, C5G7 UOX pincell nuclear reactor physics verification benchmark test case. All of the boundary conditions are reflective.

ing the volume and surface area of the geometry. Figure 5b shows the SAAF and LS equations discretised using quadratic, volume-preserved FEs. The error between the two formulations can now be observed showing that the ratio of the magnitude of the conservation error relative to the magnitude of the surface area approximation is greater. Figure 5c shows the SAAF and LS formulations discretised using IGA. Now the difference in the two formulations can be clearly observed and gives a clearer picture of the magnitude of the conservation error. This leads to the conclusion that, at least for some problems, the error induced by the lack of conservation of neutrons is small when compared to the errors caused by the approximation of geometry.

A second point of note is that the error in the numerical solutions for the non volume preserving FEM compared to the IGA differs by about six orders of magnitude for the SAAF solution. The same comparison between volume preserved FEM and IGA shows a difference of about 2-3 orders of magnitude. Whilst some of this accuracy is due to the $C^1$ inter-element continuity of the NURBS basis functions [40, 41], the main reason for this jump in accuracy is the ability of IGA to exactly represent the problem geometry.

### *5.2. Seven group, C5G7 UOX pincell lattice fission source nuclear reactor physics verification benchmark test case*

The seven-group, C5G7 UOX pincell lattice nuclear reactor physics test case has been selected to further explore the relative magnitude of errors due to the lack of conservation of neutrons and geometric approximation. Lack of conservation of neutrons has been seen to more adversely effect criticality problems so the C5G7 UOX pincell problem could be considered more taxing on the LS method [30]. The geometry of the C5G7 UOX pincell is displayed in figure 6. The cross-sections of the pin and moderator are taken from the C5G7 benchmark specification

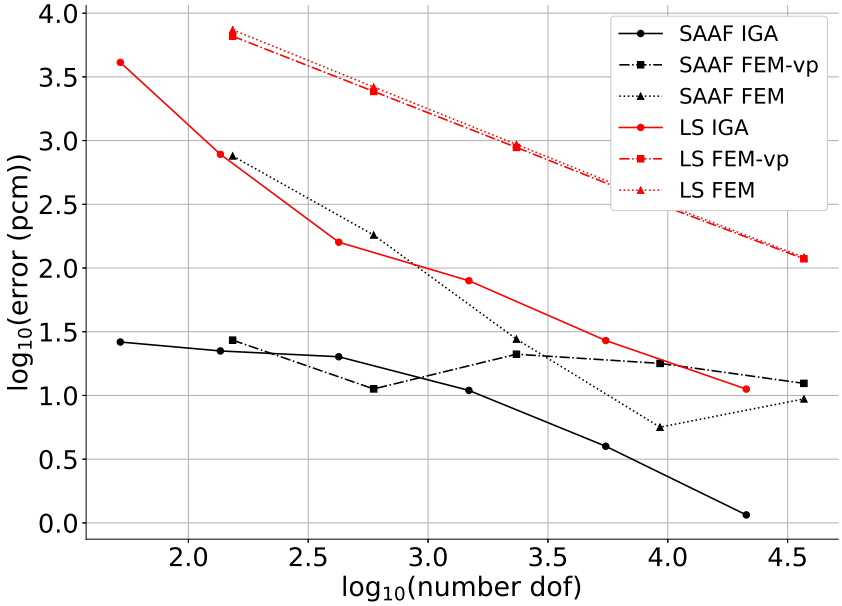


Figure 7: Error in the $K_{eff}$ for the UOX C5G7 pincell fission source nuclear reactor physics verification test case.

for materials '$UO_2$ fuel-clad' and 'moderator' respectively [50]. The transport cross-section has been used in place of the total cross-section. All of the domain boundaries are reflective to simulate an infinite lattice of pincells. This C5G7 UOX pincell test case is a criticality problem so the $K_{eff}$ will be used to investigate the magnitude of errors that arise from different discretisation methodologies and different second-order forms of the neutron transport equation.

The errors in the $K_{eff}$ using various discretisations and second order formulations for this problem can be seen in figure 7. All problems were angularly discretised using an $S_8$ quadrature set. The same general trend as was observed for the bare fuel pin test case in section 5.1 can be seen. That is, the error in the IGA solution is less than both of the FEM solutions for both the LS and SAAF formulations. However, what is more apparent here is the error caused by lack of conservation of neutrons. The $K_{eff}$ values from the LS and SAAF formulations differ by at least one order of magnitude for matching levels of spatial discretisation. The errors in the $K_{eff}$ values for the LS-FE results are of a similar order of magnitude as LS-FE results that have been presented in other works [13, 30]. However, the errors between similar SAAF-FE and LS-FE $K_{eff}$ values is much larger than the results presented in section 5.1.

It is suspected that this increase in magnitude of error is due to the following. The difference in the scalar flux and the fission source for the SAAF and LS formulations at the $i^{th}$ iteration is denoted $\phi_E^{(i)}$ and $F_E^{(i)}$. After one outer iteration $\phi_E^{(1)}$ is small and since the flux is used to generate the fission source, $F_E^{(1)}$ will also be small. However, this difference in fission sources causes a larger difference in fluxes for the second outer iteration. Therefore, $\phi_E^{(2)} > \phi_E^{(1)}$ and similarly, since $\phi_E^{(2)}$ is used to generate the fission source, $F_E^{(2)} > F_E^{(1)}$. This carries on until both solutions

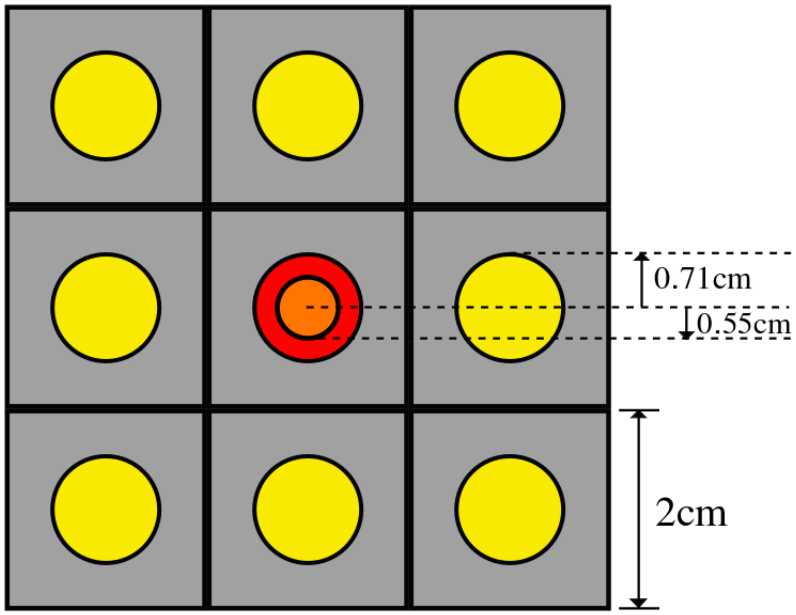


Figure 8: Geometry of BWR supercell extraneous (fixed) source nuclear reactor physics verification test case.

have converged and the final error is greater than it would be in the fixed source case.

### *5.3. BWR supercell extraneous (fixed) source nuclear reactor physics verification benchmark test case*

The boiling water reactor (BWR) supercell nuclear reactor physics test case is based on a mono-energetic, linearly anisotropic scattering problem given by Wood & Willams [51] and adapted for isotropic scattering by Owens [32]. It contains eight moderated fuel pins that surround a central pin simulating a mixture of fuel and burnable poison. The geometry specification is displayed in figure 8. All boundaries are reflective to simulate an infinite lattice. The cross-sections for the extraneous (fixed) source problem with isotropic scattering are displayed in table

| Region | Macroscopic neutron cross-section ($cm^{-1}$) | | Extraneous source strength ($cm^{-3}.s^{-1}$) |
|---|---|---|---|
| | $\sigma_t$ | $\sigma_s$ | $Q$ |
| Fuel | 0.5145 | 0.3432 | 0.0 |
| Moderator | 0.7557 | 0.7504 | 1.0 |
| Burnable poison circle | 14.270 | 0.3400 | 0.0 |
| Burnable poison annulus | 21.60 | 0.3414 | 0.0 |

Table 2: Material cross-sections for the BWR supercell extraneous (fixed) source nuclear reactor physics verification test case.

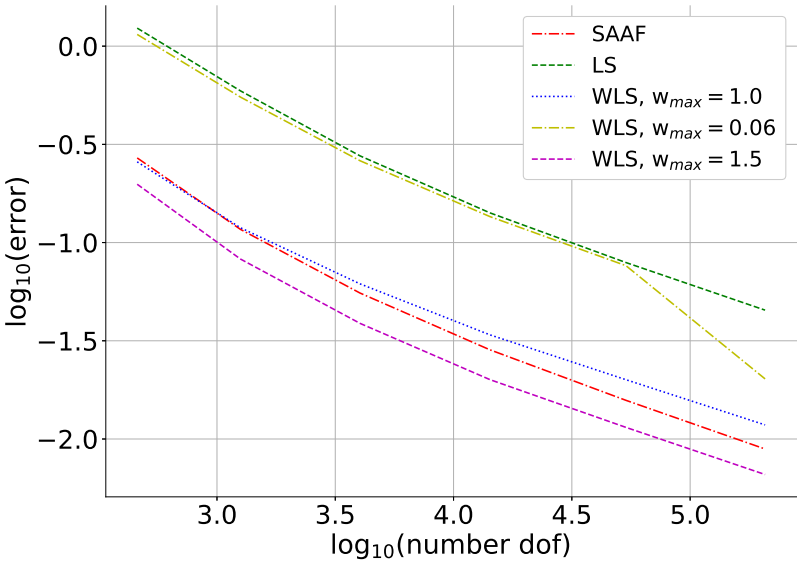


Figure 9: Error in the QoI for the BWR supercell extraneous (fixed) source nuclear reactor physics verification test case.

2. The BWR supercell nuclear reactor physics test case was selected in order to investigate how the choice of $w_{\max}$ will effect the WLS equation when applied to a realistic problem with strongly varying coefficients. The accuracy of the solution shall be investigated for the SAAF equation, the LS equation, and the WLS equation with several values of $w_{\max}$. The quantity of interest (QoI) for the BWR supercell problem is the total flux in the middle side fuel pin. The reference solution was generated using Inferno with quartic basis functions and 189,064 elements per angle.

The comparisons of the error in the QoI for the SAAF, LS, and WLS second-order forms of the neutron transport equation are show in figure 9. All results were run using ICARUS with quadratic basis functions and with $S_6$ triangular Legendre-Chebyshev angular quadrature. The WLS formulation has been run with three different weightings, $w_{\max} = 0.06, 1.0, 1.5$. These values were chosen as they cause the weighting operator to become active over different regions of the BWR supercell geometry. When $w_{\max} = 1.0$ the weighting operator will be active in the fuel and moderator regions, $w_{\max} = 1.5$ it will be active in only the moderator region, and $w_{\max} = 0.06$ it will be active in fuel, moderator, and the interior of the central pin.

In regions where the weighting operator is not active, that is $\mathcal{W} \neq w_{\max}$, the WLS formulation is identical to the SAAF formulation, up to the weak enforcement of boundary conditions. Given this, it would seem reasonable to predict that the value of $w_{\max}$ that produces a weighting operator that is active over the *smallest* part of the domain would produce results closest to the SAAF solution. Inversely, the value of $w_{\max}$ that produces a weighting operator that is active over the *largest* part of the domain would produce results furthest from the SAAF solution.

This trend can be observed in figure 9. It can also be seen that WLS formulation with $w_{\max} = 1.5$ has a lower error than the SAAF formulation at all points. This is most likely due to the

| Region | Macroscopic neutron cross-section ($cm^{-1}$) | | Extraneous source strength ($cm^{-3}.s^{-1}$) |
|---|---|---|---|
| | $\sigma_t$ | $\sigma_a$ | $Q$ |
| Absorber | 0.5 | 0.5 | 0.0 |
| Void | 0.0 | 0.0 | 0.0 |
| Source | 0.0 | 0.0 | 1.0 |

Table 3: Material cross-sections for the dog-leg duct extraneous (fixed) source radiation shielding verification test case.

error caused by the lack of conservation of neutrons in certain areas of the problem cancelling with the numerical discretisation error. The advantageous cancellation of errors may seem like a benefit. However, the inability to predict the cancellation of errors introduces uncertainty into the numerical solution. It is only clear that errors are cancelling out in the case of $w_{\max} = 1.5$ as a 'reference' SAAF solution is available. One final point that is evident from figure 9 is that the WLS solutions are superior to the LS solution for all chosen values of $w_{\max}$.

### *5.4. Dog-leg duct extraneous (fixed) source radiation shielding verification benchmark test case*

The mono-energetic dog-leg duct radiation shielding test case is taken from work done by Ackroyd [8, 52]. It consists of an extraneous (fixed) source in a voided duct surrounded by a pure absorber. Akroyd originally used the problem to investigate the efficacy of the iteration and extrapolation methods for solving second-order forms of the neutron transport equation in voided regions [8]. In this paper the dog-leg duct test case is chosen to further investigate the effect of the value of $w_{\max}$ on solutions produced by the WLS equation, in particular for voided regions. The geometry of the dog-leg duct test case can be seen seen in figure 10. The macroscopic neutron cross-sections and extraneous (fixed) source strengths are displayed in table 3. All problems are run with $S_{14}$ triangular Legendre-Chebyshev angular quadrature. The reference results were produced using Inferno, a first-order neutron transport IGA-$S_N$ code.

Figure 11 shows the errors for three different quantities of interest (QoI) defined here as:

$$I_n = \int_{V_n} \phi(\mathbf{r}) d\mathbf{r} \quad \text{for } n = 1, 2, 3, \tag{29}$$

where $V_n$ is the $n^{\text{th}}$ region shown in figure 10. The value of $w_{\max}$ is varied and for the neutron cross-section data in this problem $w_{\max} = 1$ corresponds to the source iteration compatible LS equation originally presented by Hansen [15].

In figure 11 it can be seen that increasing the value of $w_{\max}$ doesn't necessarily yield a better solution or QoI as was suggested by figure 9. A reason for this loss of accuracy in the QoI can be observed in figure 12a. It can be seen that the solution for $w_{\max} = 100$ exaggerates the peaks and troughs in the computed scalar flux. Similarly, in figure 12b the solution is over estimated over most of the line AB when $w_{\max} = 100$. Furthermore, it is noted that the sign of the error in $I_n$ for $w_{\max} = 1$ and $w_{\max} = 10$ is negative, whilst the sign of the error for $w_{\max} = 100$ is positive. This implies that there is a locally optimal value of $w_{\max}$ located at some crossover point.

To investigate this crossover point further the algorithm proposed in section 3.1 (figure 3) is applied. $I_1$ is chosen as the QoI and the first-order neutron transport equation is solved with 1920 elements per angle. Inferno is used for this calculation. Then a series of WLS calculations with the same number of elements per angle are run with varying weights until the error in $I_1$ is

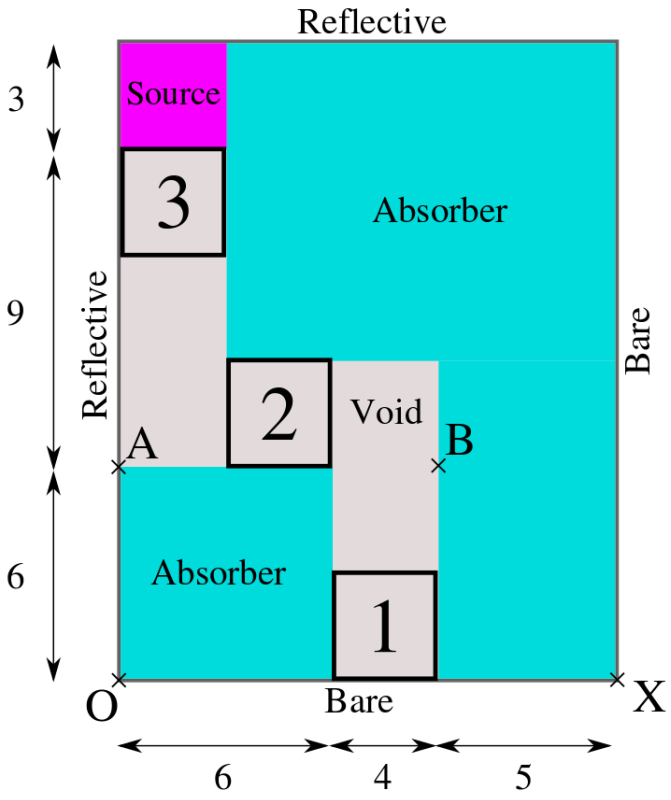


Figure 10: Geometry of the two-dimensional dog-leg duct extraneous (fixed) source radiation shielding verification test case.

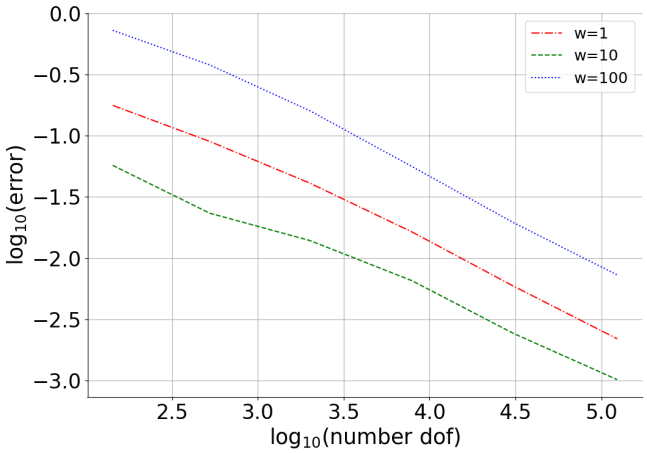


(a) Error in total flux for region 1

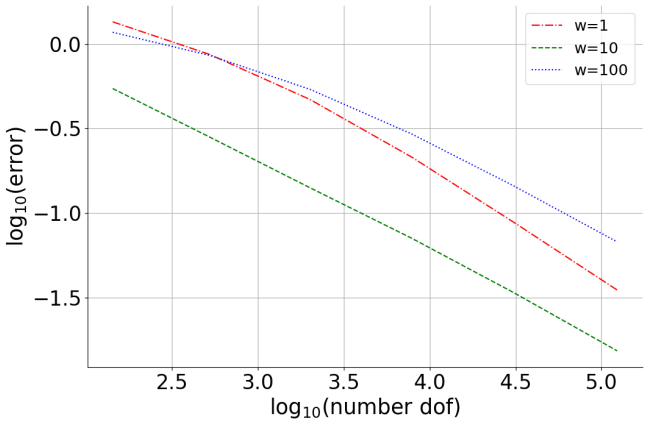


(b) Error in total flux for region 2

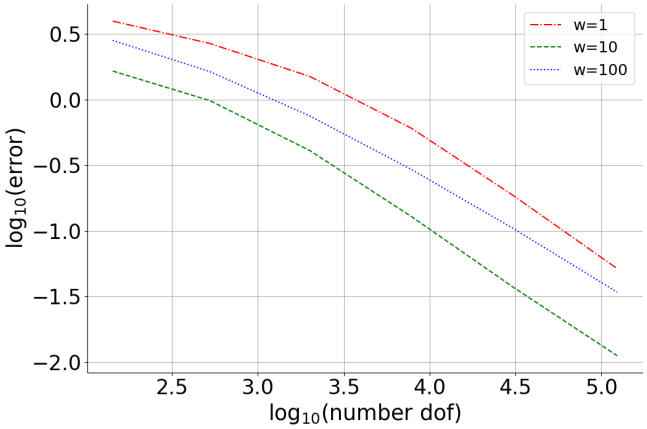


(c) Error in total flux for region 3

Figure 11: Error in various QoI for the two-dimensional dog-leg duct extraneous (fixed) source radiation shielding verification test case.

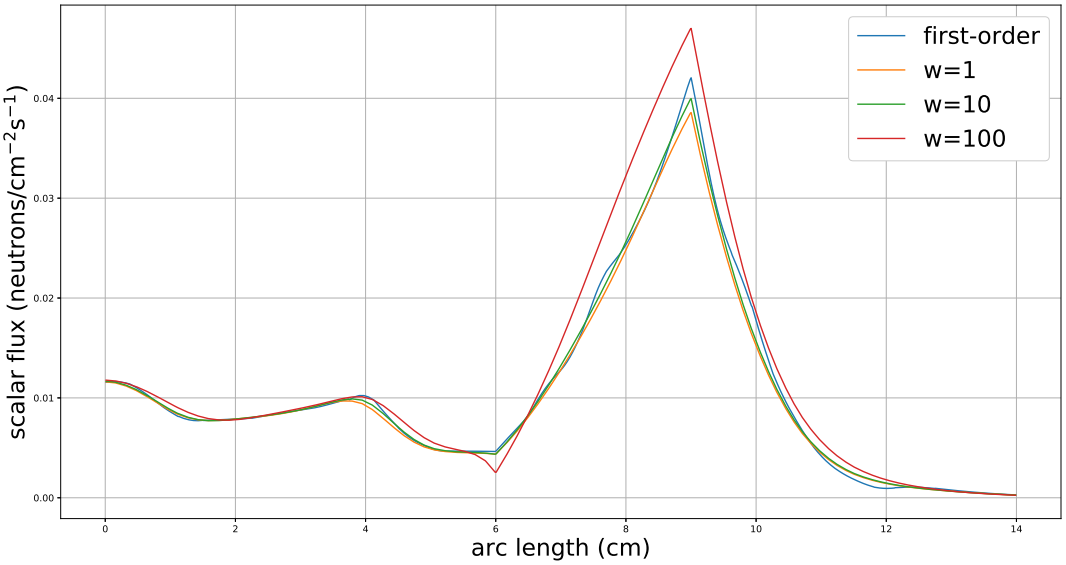


(a) Flux profile along the line OX

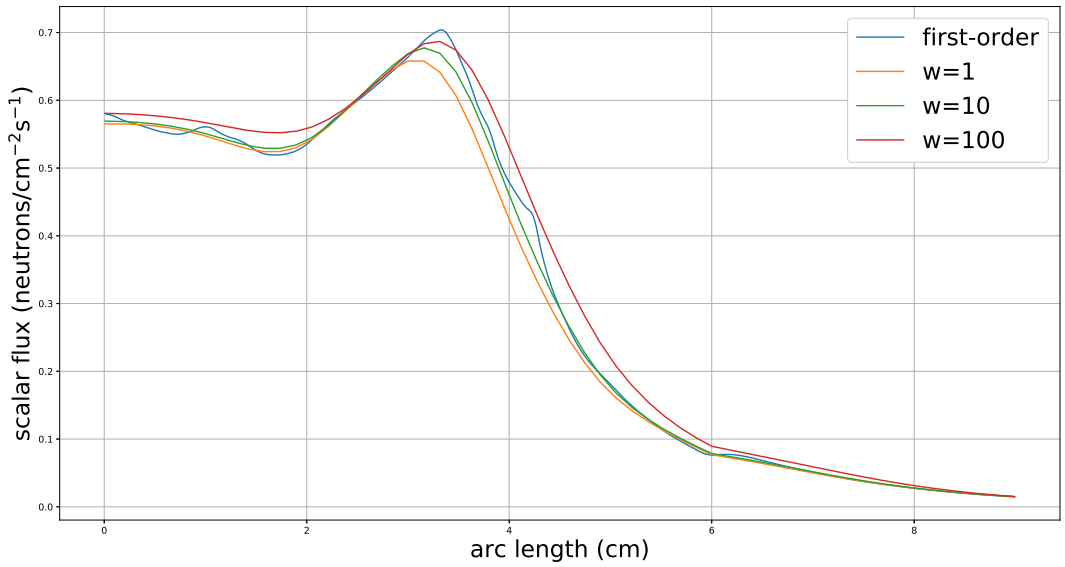


(b) Flux profile along the line AB

Figure 12: Flux profiles for the two-dimensional dog-leg duct extraneous (fixed) source radiation shielding verification test case.

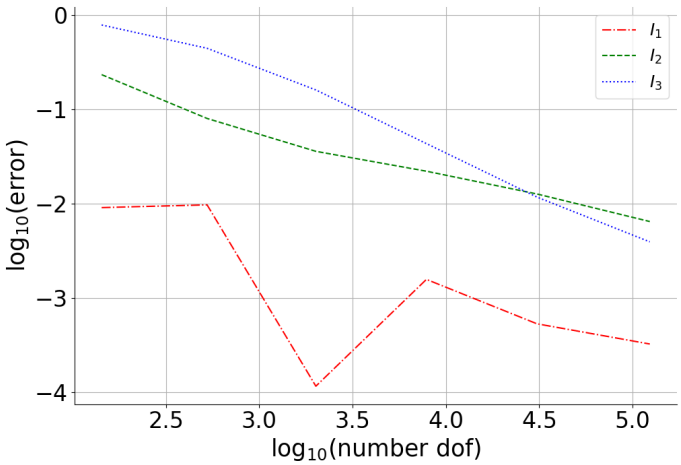


Figure 13: Error in $I_n$ with $w_{\max} = 16.8$ for the two-dimensional dog-leg duct extraneous (fixed) source radiation shielding verification test case.

| Number of elements | Value of $w_{\max}$ |
|---|---|
| 480 | 15.2 |
| 1920 | 16.8 |
| 7680 | 19.0 |

Table 4: Values of $w_{\max}$ produced by the algorithm in figure 3 for different coarse meshes applied to the two-dimensional dog-leg duct extraneous (fixed) source radiation shielding verification test case.

as small as possible. Using this method a value of $w_{\max} = 16.8$ is decided upon to one decimal place. The WLS equation is then solved over a highly refined spatial grid. All WLS solutions were calculated using the code ICARUS. The errors in all $I_n$ are displayed in figure 13.

It can be observed that for the finest mesh, with 123585 dof per angle, the errors in $I_n$ for $\forall n$ are lower than the $I_n$ calculated from other values of $w_{\max}$ with the same resolution presented in figure 11. Furthermore, it can be seen that the error in $I_1$ is clearly the lowest. This is to be expected as $I_1$ is the QoI that was used to pick the value of $w_{\max}$. The sudden dip in $I_1$ that can be observed is located at the mesh refinement level that was used to generate the reference value of $I_1$.

In order to investigate the efficacy of the algorithm presented in figure 3 two more 'coarse' meshes are chosen for the first-order calculation. The two chosen levels of refinement yield 480 elements and 7680 elements per angle for each coarse mesh. The values of $w_{\max}$ produced for each mesh are displayed in table 4. The errors in each QoI for the values of $w_{\max}$ displayed in table 4 are presented in figure 14. It can be seen that the value of $w_{\max}$ calculated from the finest 'coarse' mesh causes errors in all QoI to be the smallest. This is not unexpected as the value of $Q_f$ used in the algorithm shown in figure 3 will be more converged the finer the 'coarse' mesh is. This means that the matching performed in the algorithm is against a more converged QoI. However, this does not necessarily imply that the optimal value of $w_{\max}$ changes with mesh

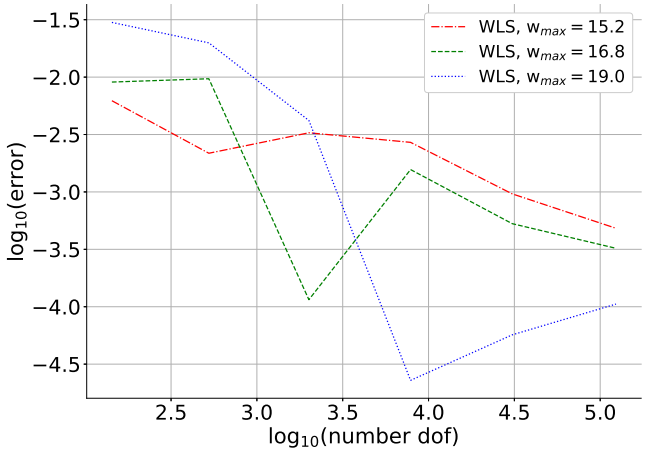


(a) Error in $I_1$

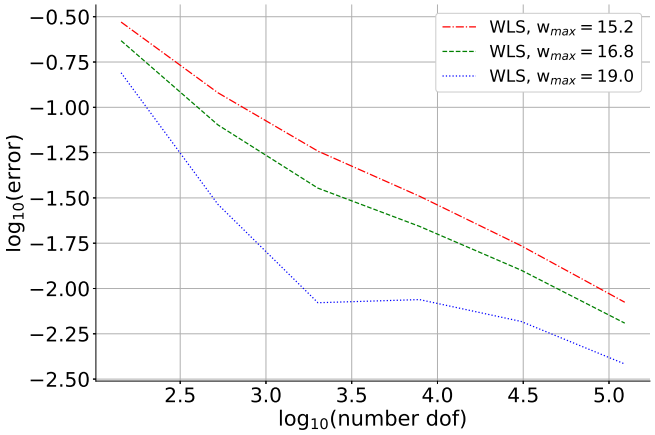


(b) Error in $I_2$

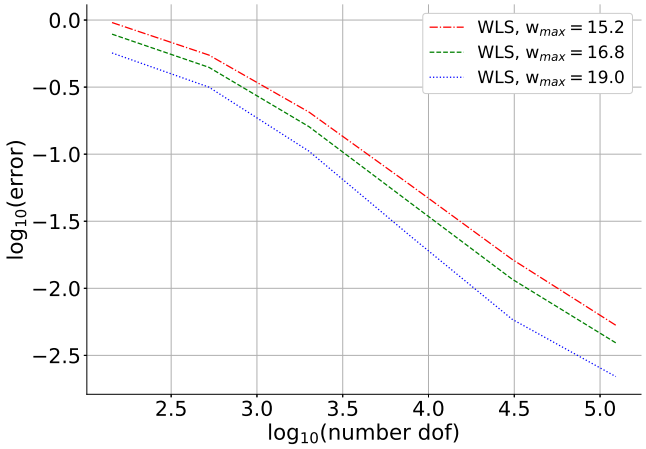


(c) Error in $I_3$

Figure 14: Error in various QoI for the two-dimensional dog-leg duct extraneous (fixed) source radiation shielding verification test case for values of $w_{\max}$ selected using the algorithm in figure 3.

refinement in two-dimensions. Further investigation is necessary to determine that.

It can be seen that the methodology presented in section 3.1 is useful for choosing the value of $w_{\max}$ for use in the WLS equation when solving problems involving voided regions, particularly where a given QoI is desired. The computational cost of applying this algorithm can be kept low by choosing a sufficiently coarse mesh. However, figure 14 suggests that using a finer coarse mesh for the first-order transport solution leads to a value of $w_{\max}$ that is closer to optimal.

## 6. Conclusion

In this paper the weighted least squares (WLS) neutron transport equation was derived and spatially discretised using non-uniform rational B-spline (NURBS) based isogeometric analysis (IGA). The angular domain was discretised using the discrete ordinate ($S_N$) method. IGA is a spatial discretisation technique that is able to exactly represent the volume and surface area of geometries that can be created using commercial CAD software. This includes conic sections in two-dimensions (2D) and quadric surfaces in three-dimensions (3D).

The WLS formulation is an elliptic second-order form of the neutron transport equation. It can be solved over voided regions and is compatible with the source iteration method. The WLS equation involves two weighting parameters. The first is used as a penalty parameter to weakly impose boundary conditions whilst the second is used to weight voided regions of the problem domain. For the correct choices of these weighting parameters the WLS equation is equivalent to the self-adjoint angular flux (SAAF) form of the neutron transport equation for non-voided problems. Therefore, the WLS equation conserves neutrons in non-voided regions of the domain. However, in voided regions the choice of $w_{\max}$ can significantly impact the solution due to lack of conservation of neutrons and the impact on the causality of the WLS formulation [30].

In an attempt to ameliorate the error in voided regions, a methodology for choosing a value of $w_{\max}$ that involves solving the first-order neutron transport equation over a coarse mesh was presented. This algorithm is computationally inexpensive compared to solving the WLS on a fine mesh.

Several nuclear reactor physics and radiation shielding verification benchmark test cases were selected to evaluate the impact of two factors on the error in the solution: the effect of using a NURBS based IGA discretisation, and the effect the choice of $w_{\max}$ can have on two-dimensional problems. A single-group, extraneous (fixed) source bare fuel pin problem and an OECD/NEA seven-group, two-dimension C5G7 UOX pincell fission source problem were discretised using IGA and the FE method. The source iteration compatible least square (LS) equation and the SAAF equation were solved for both of these discretisations. The LS equation is a particular case of the WLS equation. It was shown that the error due to the geometric approximation inherent in the FE discretisation was of a larger magnitude than the error due to lack of conservation of neutrons for the bare fuel pin problem. For the fission source problem the two errors were of roughly equal magnitudes.

The effect of the value of $w_{\max}$ on a selected QoI was investigated using a non-void two-dimensional boiling water reactor (BWR) supercell nuclear reactor physics test case. It was found that the greater the area of the domain where $\mathcal{W} = w_{\max}$ the closer the solution of the WLS equation was to the solution of the LS equation. Inversely, the greater the area of the domain where $\mathcal{W} = \frac{1}{\sigma_t}$ the closer the solution of the WLS equation was to the solution of the SAAF equation. Furthermore, a two-dimensional dog-leg duct radiation shielding test case that included a voided duct region was used to investigate the efficacy of the methodology presented

to select the value of $w_{\max}$. The methodology involves using a coarse solution to the first-order transport equation. It was shown that the finer the coarse solution was, the more suitable the value of $w_{\max}$ generated.

Overall the IGA spatial discretisation method seems a promising numerical discretisation scheme, mostly due to its ability to exactly represent conic sections in two-dimensions and quadric surfaces in three-dimensions, but also due to the high inter-element continuity of the NURBS basis functions within a NURBS patch. Furthermore, the methodology presented for selecting $w_{\max}$ could enable the effective use of the WLS equation for a wide variety of voided problems. Future work could include making the value of $w_{\max}$ spatially or angularly dependent over the problem domain in 2D. A methodology for selecting such a $w_{\max}(\mathbf{r}, \mathbf{\Omega})$ would also need to be defined. Further research is required to extend the IGA-WLS method to three-dimensional nuclear reactor physics and radiation shielding problems as well as incorporate energy-dependent, spatially adaptive meshes. As the geometry of the computational domain is always represented exactly using IGA, even on the coarsest spatial representation, this enables spatial refinement to performed at run-time without the need for any complex unstructured re-meshing algorithms or external meshing programs. Therefore, a locally refined IGA discretisation methodology, coupled with a suitable goal-based adaptive mesh refinement algorithm, could potentially improve the numerical accuracy per dof as well as the computational efficiency compared to other unstructured mesh numerical discretisation schemes.

**Acknowledgements**

C. Latimer would like to acknowledge the Engineering and Physical Sciences Research Council (EPSRC) through the Doctoral Training Award (DTA) PhD scheme and their knowledge transfer secondment (KTS) programme (EPSRC impact acceleration award grant reference number: EP/R511547/1) and also the industrial support of Rolls-Royce. M. D. Eaton and J. Kópházi would like to thank the EPSRC for their support through the following grants: Adaptive Hierarchical Radiation Transport Methods to Meet Future Challenges in Reactor Physics (EPSRC Grant No.: EP/ J002011/1) and RADIANT: A Parallel, Scalable, High Performance Radiation Transport Modelling and Simulation Framework for Reactor Physics, Nuclear Criticality Safety Assessment and Radiation Shielding Analyses (EPSRC Grant No.: EP/K503733/1). Finally, the authors would like to thank the high performance computing (HPC) service support team at Imperial College London.

[1] J. Spainer and E. M. Gelbard. *Monte Carlo Principles and Neutron Transport Problems*. Dover Publications, 2nd edition, 2008.

[2] K. Ueki and P. N. Stevens. Variance Reduction Techniques Using Adjoint Monte Carlo Method in Shielding Problem. *Journal of Nuclear Science and Technology*, 16(2):117–131, 1979.

[3] T. M. Evans, A. S. Stafford, R. N. Slaybaugh, and K. T. Clarno. Denovo: A New Three-Dimensional Parallel Discrete Ordinates Code in SCALE. *Nuclear Technology*, 171:171–200, 2010.

[4] H. A. Van Der Vorst and K. Dekker. Conjugate gradient type methods and preconditioning. *Journal of Computational and Applied Mathematics*, 24:73–87, 1988.

[5] M. Hanus and R. G. McClarren. On the use of symmetrized transport equation in goal-oriented adaptivity. *Journal of Computational and Theoretical Transport*, 0(0):1–20, 2016.

[6] V. S. Vladimirov. Mathematical problems in the one-velocity theory of particle transport. Technical Report AECL-1661, Atomic Energy of Canada Ltd., Chalk River, Ontario, January 1963.

[7] J. E. Morel and J. M. McGhee. A self-adjoint angular flux equation. *Nuclear Science and Engineering*, 132:312–325, 1999.

[8] R. T. Ackroyd and N. S. Riyait. Iteration and extrapolation methods for the approximate solution of the even-parity transport equation for systems with voids. *Annals of Nuclear Energy*, 16(1):1–32, 1989.

[9] C. R. E. de Oliveira, M. D. Eaton, A. P. Umpleby, and C. C. Pain. Finite Element-Spherical Harmonics Solutions of the 3D Kobayashi Benchmarks with Ray-Tracing Void Treatment. *Progress in Nuclear Energy*, 2001.

[10] R. T. Ackroyd and D. T. Grenfell. A Finite Element Method for Neutron Transport III. Two-Dimensional One-Group Test Problems. *Annals of Nuclear Energy*, 6:563–577, 1979.

[11] R. T. Ackroyd, J. G. Issa, and N. S. Riyait. Treatment of voids in finite element transport methods. *Progress in Nuclear Energy*, 18:85–89, 1986.

[12] Y. Wang, H. Zhang, and R. C. Matrineau. Diffusion acceleration schemes for self-adjoint angular flux formulation with a void treatment. *Nuclear Science and Engineering*, 176:201–225, 2014.

[13] V. M. Laboure, R. G. McClarren, and Y. Wang. Globally Conservative, Hybrid Self-Adjoint Angular Flux and Least-Squares Method Compatible with Voids. *Nuclear Science and Engineering*, 185:294–306, February 2017.

[14] W. Zheng, R. G. McClarren, and J. E. Morel. An Accurate Globally Conservative Subdomain Discontinuous Least-Squares Scheme for Solving Neutron Transport Problems. *Nuclear Science and Engineering*, 189:259–271, 2018.

[15] J. Hansen, J. Peterson, J. Morel, J. Ragusa, and Y. Wang. A Least-Squares Transport Equation Compatible with Voids. *Journal of Computational and Theoretical Transport*, 43:374–401, 2014.

[16] J. Brannick, C. Ketelsen, T. Manteuffel, and S. McCormick. Least-squares finite element methods for quantum electrodynamics. *SIAM Journal of Scientific Computing*, 32(1):398–417, 2010.

[17] J. J. Heys, E. Lee, T. A. Manteuffel, and S. F. McCormick. An alternative least-squares formulation of the Navier-Stokes equations with improved mass conservation. *Journal of Computational Physics*, 226:994–1006, 2007.

[18] S. D. Bond, J. H. Chaudhry, E. C. Cyr, and L. N. Olsen. A First-Order System Least-Squares Finite Element Method for the Poisson-Boltzmann Equation. *Journal of Computational Chemistry*, 31:1625–1635, 2009.

[19] R. T. Ackroyd. Least-Squares Derivation of Extremum and Weighted-Residual Methods for Equations of Reactor Physics - I. The First-Order Boltzmann Equation and a First-Order Initial-Value Equation. *Annals of Nuclear Energy*, 10:65–99, 1983.

[20] S. L. Schofield. A Maximum Principle for the First-Order Boltzmann Equation, Incorporating a Potential Treatment of Voids. *Annals of Nuclear Energy*, 15(12):543–551, 1988.

[21] S. L. Schofield and M. Pourzand. Single-pass treatment of voids in F.E. transport theory. *Progress in Nuclear Energy*, 25(2-3):217–229, 1991.

[22] S. L. Schofield and R. T. Ackroyd. A Maximum Principle for Time Dependent Transport in Systems with Voids. *Annals of Nuclear Energy*, 23(7):567–574, 1996.

[23] T. Manteuffel and K. Ressel. Least-squares finite-element solution of the neutron transport equation in diffusive regimes. *Society for Industrial and Applied Mathematics*, 35(2):806–835, April 1998.

[24] E. Varin and G. Samba. Spherical harmonics finite element transport equation solution using a least-squares approach. *Nuclear Science and Engineering*, 151:167–183, 2005.

[25] T. M. Austin and T. A. Manteuffel. A least-squares finite element method for the linear Boltzmann equation with anisotropic scattering. *SIAM Journal of Numerical Analysis*, 44(2):540–560, 2006.

[26] J. H. Chaudhry, E. C. Cyr, K. Liu, T. A. Manteuffel, L. N. Olson, and L. Tang. Enhancing least-squares finite element methods through a quantity-of-interest. *SIAM Journal of Numerical Analysis*, 52(6):3085–3105, 2014.

[27] C. Drumm. Spherical Harmonics ($P_N$) Methods in the SCEPTRE Radiation Transport Code. In *ANS M&C2015 - Joint International Conference on Mathematics and Computation (M&C), Supercomputing in Nuclear Applications (SNA) and the Monte Carlo (MC) Method*. Nashville, TN, USA, April 2015.

[28] C. Ketelsen, T. Manteuffel, and J. B. Schroder. Least-squares finite element discretization of the neutron transport equation in spherical geometry. *SIAM Journal of Scientific Computing*, 37(5):S71–S89, 2015.

[29] V. M. Laboure, Y. Wang, and M. D. DeHart. Least-Squares $P_n$ Formulation of the Transport Equation Using Self-Adjoint-Angular-Flux Consistent Boundary Conditions. In *PHYSOR 2016 - Unifying Theory and Experiments in the 21st Century*, INL/CON-15-36402, Sun Valley, Idaho, USA, May 2016.

[30] H. R. Hammer, J. E. Morel, and Y. Wang. A Weighted Least-Squares Transport Equation Compatible with Source Iteration and Voids. *Nuclear Science and Engineering*, 193:388–403, 2018.

[31] S. K. Hall, M. D. Eaton, and M. M. R. Williams. The Application of Isogeometric Analysis to the Neutron Diffusion Equation for a Pincell Problem with an Analytic Benchmark. *Annals of Nuclear Energy*, 49:160–169, 2012.

[32] A. R. Owens, J. A. Welch, J. Kópházi, and M. D. Eaton. An adaptive, hanging-node, discontinous isogeometric analysis method for the first-order form of the neutron transport equation with discrete ordinate ($S_N$) angular discretisation. *Computer Methods in Applied Mechanics and Engineering*, 318:215–241, 2017.

[33] C. Hofreither and S. Takacs. Robust multigrid for isogeometric analysis based on stable splittings of spline spaces. *SIAM Journal of Numerical Analysis*, 55(4):2004–2024, 2017.

[34] Y. Bazilevs, V. M. Calo, J. A. Cottrell, J. E. Evans, T. J. R. Hughes, S. Lipton, M. A. Scott, and T. W. Sederberg. Isogeometric analysis using T-splines. *Computer Methods in Applied Mechanics and Engineering*, 199:229–263, 2010.

[35] K. A. Johannessen, T. Kvamsdal, and T. Dokken. Isogeometric analysis using LR B-splines. *Computer Methods in Applied Mechanics and Engineering*, 269:471–514, 2014.

[36] R. R. Hiemstra, F. Calabro, D. Schillinger, and T. J. R. Hughes. Optimal and Reduced Quadrature Rules for Tensor Product and Hierachically Refined Splines in Isogeometric Analysis. *Computer Methods in Applied Mechanics and Engineering*, 316:966–1004, 2017.

[37] T. J. R. Hughes, J. A. Cottrell, and Y. Bazilevs. *Isogeometric Analysis: Toward Integration of CAD and FEA*. John Wiley and Sons, 2009.

[38] L. Piegl. On NURBS: A Survey. *IEEE Computer Graphics and Applications*, 11:55–71, 1991.

[39] L. Piegl and W. Tiller. *The NURBS Book 2nd edition*. Springer-Verlag, 1997.

[40] J. Welch, J. Kópházi, A. R. Owens, and M. D. Eaton. A geometry preserving, conservative, mesh-to-mesh isogeometric interpolation algorithm for spatial adaptivity of the multigroup, second-order even-parity form of the neutron transport equation. *Journal of Computational Physics*, 347:129–146, August 2016.

[41] J. A. Welch, J. Kópházi, A. R. Owens, and M. D. Eaton. Isogeometric analysis for the multigroup neutron diffusion equation with applications in reactor physics. *Annals of Nuclear Energy*, 101:465–480, 2017.

[42] L. Beirao da Veiga, L. F. Pavarino, S. Scacchi, O. B. Widlund, and S. Zampini. Isogeometric BDDC preconditioners with deluxe scaling. *Journal of Scientific Computation*, 36(3):1118–1139, 2014.

[43] C. Latimer, J. Kópházi, and M. D. Eaton. Isogeometric multi-level iterative solution algorithms with applications in nuclear reactor physics. In *Proceedings of the 2018 26th International Conference on Nuclear Engineering*, volume 3, London, UK, 2018.

[44] X. Zhou. $G^2$ continuity algorithms between adjacent NURBS patches along common cubic boundary curve. *Chinese Journal of Aeronautics*, 16(4):241–246, 2003.

[45] V. M. Laboure. *Improved Fully-Implicit Spherical Harmonics Methods for First and Second Order Forms of the Transport Equation using Galerkin Finite Element*. PhD thesis, Texas A & M University, August 2016.

[46] J .T. Oden and J. N. Reddy. *An Introduction to the Mathematical Theory of Finite Elements*. Dover Publications, 1976.

[47] J. Y. Moller and J. J. Lautard. MINARET, a Deterministic Neutron Transport Solver for Nuclear Core Calculations. In *International Conference on Mathematics and Computational Methods Applied to Nuclear Science and Engineering*, Rio de Janiro, Brazil, May 2011.

[48] A. R. Owens, J. A. Welch, J. Kópházi, and M. D. Eaton. Discontinuous isogeometric analysis methods for the first-order form of the neutron transport equation with discrete ordinate ($S_N$) angular discretisation. *Journal of Computational Physics*, 315:501–535, 2016.

[49] A. R. Owens, J. Kópházi, J. A. Welch, and M. D. Eaton. Energy dependent mesh adaptivity of discontinous isogeometric discrete ordinate methods with dual weighted residual error estimators. *Journal of Computational Physics*, 335:352–386, 2017.

[50] E. E. Lewis, G. Palmiotti, T. A. Taiwo, M. A. Smith, and N. Tsoulfanidis. Benchmark on Deterministic Transport Calculations Without Spatial Homogenisation - A 2-D/3-D MOX Fuel Assembly Benchmark. *Nuclear Science*, 2003.

[51] J. Wood and M. M. R. Williams. Recent Progress in the Application of the Finite Element Method to the Neutron Transport Equation. *Progress in Nuclear Energy*, 14(1):21–40, 1984.

[52] R. T. Ackroyd. *Finite Element Methods for Particle Transport: Applications to Reactor and Radiation Physics*. John Wiley & Sons, 1997.